Sensitivities of Tropical Pacific Precipitation Simulations to Physical Parameters in CAM6 and Implications for AGCMs

Lin Chen[1]*†, Yesheng Zhu[1†], Yong Wang[2], Haoqian Li[1], De-Zheng Sun[3], Ming Sun[4], Huiping Yan[1], Yongqiang Yu[5]

[1] State Key Laboratory of Climate System Prediction and Risk Management/Key Laboratory of Meteorological Disaster, Ministry of Education/Collaborative Innovation Center on Forecast and Evaluation of Meteorological Disasters, Nanjing University of Information Science and Technology, Nanjing, China

[2] Department of Atmospheric and Oceanic Sciences and Institute of Atmospheric Sciences, Fudan University, Shanghai, China

[3] Nanjing-Helsinki Institute in Atmospheric and Earth System Sciences, Nanjing University-Suzhou Campus, Suzhou, Jiangshu, China

[4] Anhui Climate Center, Hefei, China

[5] State Key Laboratory of Earth System Numerical Modeling and Application, Institute of Atmospheric Physics, Chinese Academy of Sciences, Beijing, China

*Corresponding author: Lin Chen (chenlin@nuist.edu.cn)

† Lin Chen and Yesheng Zhu contributed equally to this work.

Key Points:

- Two convective parameters and three cloud ice parameters are identified as crucial for simulating tropical Pacific precipitation in CAM6
- Nonlinear effects of parameters are critical for mean precipitation simulation and an interpretation of underlying processes is provided
- Some biases in simulating precipitation in PPE experiments align with that in AMIP simulations, offering implications for advancing AGCMs

Abstract

In this study, we examined the key parameters within deep convection scheme and cloud physics scheme of the CAM6 model to ascertain their significance and influence on simulating mean precipitation in the tropical Pacific. Through simultaneously perturbing twelve selected parameters from deep convection and cloud physics schemes, we conducted perturbed parameter ensemble (PPE) experiments with 128 members. Our analysis uncovered that the parameters showing the most influential effects on tropical Pacific precipitation simulations can be separated into two distinct categories: those primarily governed by the convection scheme, which reflects the competition between convective and large-scale precipitation, and those predominantly influenced by cloud ice processes. Furthermore, we revealed the importance of nonlinear effects of these perturbed parameters on the simulation of mean precipitation and interpreted the underlying mechanisms. Some biases in simulating precipitation revealed by our PPE experiments align with those in AMIP simulations, offering valuable insights for the AGCM's advancement.

Plain Language Summary

Tropical precipitation is a critical component of the Earth's climate system, influencing energy redistribution, radiative forcing, atmospheric circulation, water cycle, and various biogeochemical processes. However, the state-of-the-art atmospheric models still exhibit persistent errors in simulating tropical precipitation. Utilizing the Community Atmosphere Model version 6 (CAM6) as an experimental platform, we implemented a perturbed parameter ensemble (PPE) approach to identify key factors affecting the simulation skill of tropical precipitation. Through the PPE experiments and statistical analyses, we pinpointed several key parameters within the model's atmospheric parameterization schemes that are pivotal and potentially tunable to reduce the bias in precipitation simulations. This research offers valuable insights that are informative for the development of the atmospheric general circulation models.

1. Introduction

Tropical precipitation is a critical component of the Earth climate system, affecting energy redistribution, radiative forcing, atmospheric circulation, water cycle, and various biogeochemical processes, with far-reaching effects on global and regional climate (Meehl et al., 2007; Allan et al., 2010; Stephens et al., 2010; Trenberth et al., 2011; Fläschner et al., 2016; Wang et al., 2021).

General circulation models (GCMs) are vital for climate research but still shows some distortions regarding accurately simulating the tropical mean precipitation and sea surface temperature (SST) (e.g., Lin, 2007; Li and Xie, 2014; Wang et al., 2014; Chen et al., 2019; Ge and Chen, 2020; He et al., 2023; Ma and Yang, 2020; Ma and Jiang, 2020). A major issue is the long-standing Double Intertropical Convergence Zone (ITCZ) bias (Lin, 2007; Stouffer et al., 2017). This bias manifests as an overestimation of precipitation in the South Pacific Convergence Zone (SPCZ) by most coupled GCMs, resulting in erroneous parallel rain belts straddling the equator (Mechoso et al., 1995; Kirtman et al., 2002; Dai, 2006; Zhang & Song, 2010; Tian, 2015). Both CMIP5 and CMIP6 show an overall positive bias in tropical Pacific precipitation (Song & Zhang, 2009; Liu &Kevin, 2023; Zhou et al., 2020). Another remarkable bias in the coupled GCMs is the excessive cold tongue bias (Mechoso et al., 1995; Chen el al. 2013). It is well accepted that the double-ITCZ bias is closely associated to the cold bias in SST (Lin, 2007; Li and Xie, 2012, 2014), and both the atmospheric precipitation bias and the oceanic SST bias can deteriorate each other via air-sea coupling, posing the challenging to identify the causal relationship between these two major biases in coupled GCMs (Chen et al., 2013).

To understand and reduce the simulation biases regarding the tropical precipitation and SST in coupled GCMs, one strategy is to improve the simulation skill of tropical precipitation from the perspective of atmosphere-only GCMs (AGCMs). Indeed, the representation of the convection and cloud physical processes is one of the significant sources of tropical climate simulation biases (Zhang and McFarlane, 1995; Morrison and Gettelman, 2008; Li et al., 2014; Zhang et al., 2024). Most models apply the physical parameterization schemes to simulate these sub-grid processes based on assumptions or approximations (Manabe et al., 1965; Donner et al., 2001; Arakawa, 2004). After decades of efforts, the physical parameterization schemes have made significant progress. Nonetheless, the scarcity of observational data and the intricacy of

the underlying physical processes introduce considerable uncertainty into the values of the empirical parameters within the schemes, contaminating the tropical precipitation simulations (Murphy et al., 2004; Her et al., 2019). Currently, tuning the uncertain parameters within the physical parameterization scheme stands out as one of the most promising ways to further refine the physical parameterization scheme.

While previous studies have examined the effects of physical parameters on precipitation simulation, further study is needed. For instance, the significance of nonlinear effect in the process of parameter adjustment remains debated. Some studies suggest that nonlinear effect such as the interaction between parameters is important (Fowler et al., 1996; Zhang et al., 2023), while others argue that the nonlinear effect seems to be not important (Qian et al., 2015, Yang et al., 2023). Therefore, it is worthwhile to further investigate whether the nonlinear interaction between parameters has a substantial impact on the simulation of tropical precipitation. This could provide scientific evidence to clarify whether the nonlinear interaction between parameters should be considered when optimizing parameters.

Perturbed parameter ensemble (PPE) is an approach used to study the sensitivity of model parameters by systematically altering parameters and conducting experiments to assess the model simulations' responses. The most straightforward form of this method, single-parameter perturbation, involves perturbing one parameter in a set of experiments (Li et al., 2013; Schiro et al., 2019), but this lacks the capacity to examine the parameter interactions. To overcome this limitation, some studies adopt the multi-parameter perturbation strategy to delve into the impacts of physical parameters on simulations. This strategy entails simultaneously perturbing multiple parameters and then pinpointing the simulation sensitivity through assessing the reduction in the residual sum of squares attributable to each parameter. This method is capable of quantifying the parameter interactions, including higher-order effects. For instance, Hou et al. (2012) conducted experiments by simultaneously perturbing ten selected parameters, revealing the significance of hydrologic parameters on surface flux simulations to hydrologic parameters in CLM4. Zhao et al. (2013) perturbed sixteen uncertain parameters in CAM5 and found that the autoconversion size threshold for ice to snow (*dcs*) emerges as the most influential parameter affecting the net radiation fluxes. Guo et al. (2014) conducted an analysis

115 of cloud simulations by simultaneously perturbing sixteen parametersin the single-column
116 version of CAM5, uncovering that only a few tunable parameters account for the majority of
117 variance in cloud properties. Xie et al. (2023) perturbed nine moist physical parameters to
118 quantify the parametric uncertainty on the simulation of tropical cloud fraction. Zhang et al.
119 (2023) evaluated the impact of the perturbed parameters on the Asian summer monsoon in the
120 HadGEM3-GC3.05 model, and identified four cloud physics and aerosols parameters showing
121 the most influential effects on the precipitation simulation.

122 Recently, the latest version of the Community Atmosphere Model—CAM6 has been
123 released. CAM6 is a sophisticated AGCM, serving as the atmospheric component of the widely-
124 used Community Earth System Model (CESM, Danabasoglu et al., 2020). In CAM6, the latest
125 cloud microphysics scheme—Morrison-Gettelman (MG2, Gettelman and Morrison, 2015) is
126 applied, and the Zhang-McFarlane deep convection scheme (Zhang and McFarlane, 1995) has
127 also undergone structural adjustments and algorithm optimization. Although a PPE method was
128 applied to CAM6 to explore climate sensitivity to atmospheric physics parameters (Eidhammer
129 et al., 2024; Gettelman et al., 2024; Duffy et al., 2024), so far only few studies have focused on
130 the influence of the updated parameterization schemes in CAM6 on the tropical precipitation
131 simulation. Furthermore, most of the previous studies paid more attention to the adjustment of
132 parameters, without elucidating the underlying physical mechanisms behind the key parameters.
133 Therefore, this study aims to examine the impacts of the parameter uncertainty in the convective
134 and cloud microphysics schemes on tropical precipitation simulation, through employing
135 CAM6 as an experimental platform. The goal is to identify critical parameters that have the
136 most influential effects on tropical precipitation and to provide the interpretation of their
137 impacts, thereby yielding the implications for the advancements of other CGCMs.

138 # 2. Datasets and methodology

139 ## 2.1 Observational datasets and CMIP6 Data

140 The observational datasets used in this study include (1) SST data from HadISST (Rayner
141 et al., 2003), which has a horizontal resolution of 1°×1° and covers 1979–2014; (2) precipitation
142 data from Global Precipitation Climatology Project (GPCP) (Adler et al., 2003), which has a
143 horizontal resolution of 2.5°×2.5° and covers 1979–2014; (3) convective and large-scale

144 precipitation from the TRMM-3A25 dataset, which has a horizontal resolution of 0.5°
145 resolution and covers 1998–2014 (Kozu et al., 2001; for more details about the convective
146 versus large-scale precipitation in TRMM, see Text S1).

147 The Atmospheric Model Intercomparison Project (AMIP) simulations covering 1979–
148 2014 from thirty Coupled Model Intercomparison Project Phase 6 (CMIP6; Eyring et al., 2016)
149 models are also utilized. For more details about these CMIP6 models, please refer to Table S1.

150 **2.2 CAM6 Model**

151 The Community Atmosphere Model version 6 (CAM6) is the latest atmospheric
152 component of Community Earth System Model version 2 (CESM2). CAM6 incorporates an
153 advanced two-moment bulk microphysics scheme by Morrison and Gettelman (MG2,
154 Gettelman and Morrison, 2015). In CAM6, the cloud microphysics scheme has been improved
155 from MG1 to MG2. Compared to MG1, the improvements in MG2 include changing the
156 diagnostic precipitation to prognostic precipitation, thereby reducing numerical instability and
157 enabling the simulation of the continuous dynamic evolution of precipitation (Gettelman and
158 Morrison, 2015). The deep convection scheme adopted in CAM6 is the Zhang-McFarlane
159 convection scheme (Zhang and McFarlane, 1995), which is a parameterization scheme that
160 considers the impact of entrainment on the vertical variation of Convective Available Potential
161 Energy (CAPE) (Neale et al., 2008), as well as momentum transport (Richter and Rasch, 2008).
162 In CAM6, Zhang-McFarlane scheme has also undergone structural adjustments and algorithm
163 optimizations, including a transition from employing the Newton method to utilizing the Brent
164 method for solving equations.

165 **2.3 Methodology**

166 **2.3.1 Perturbed Parameter Ensemble**

167 Following Qian et al. (2015) and Schiro et al. (2019), we selected twelve deep convection
168 and cloud physics parameters (refer to Table S2) to conduct the PPE experiments. These twelve
169 parameters were perturbed within the prescribed ranges based on the observation and/or the
170 expert judgment from model developers who possess experience in running the model at a range
171 of parameter values.

172 Using quasi-Monte Carlo (QMC) sampling, we systematically perturbed twelve

parameters related to deep convective and cloud physics, yielding 128 distinct parameter configurations for the PPE experiments. Such approach facilitates a more efficient traversal of the high-dimensional parameter space (see Text S2 for details). For comparison with AMIP simulation, each member in the PPE experiments was integrated for the period of 1979–2014.

2.3.2 Generalized Linear Model (GLM)

The GLM approach is employed to examine the sensitivity of the precipitation simulation to the perturbed parameters. This analysis includes assessing the linear effects of the parameters, represented by ($\sum_{j=1}^{n} \beta_j * p_j$) and the nonlinear interactions, encapsulated by ($\sum_{j=1}^{n} \sum_{k=1}^{n} \beta_{j,k} * p_j * p_k$). The model structure of GLM is as follows:

$$Y = \beta_0 + \sum_{j=1}^{n} \beta_j * p_j + \sum_{j=1}^{n} \sum_{k=1}^{n} \beta_{j,k} * p_j * p_k + \varepsilon, \varepsilon \sim N(0, \sigma^2) \quad (1),$$

where Y represents the response variable; p_j is the jth parameter, β_j and $\beta_{j,k}$ are the coefficients of the linear and second-order nonlinear interaction terms, respectively; ε denotes the residual term. The relative contributions of each parameter and the nonlinear term are quantified by assessing the reduction in the residual sum of squares caused by each term (Guo et al., 2014; Qian et al., 2015).

3. Results

3.1 Overall simulation performance of 128 PPE members

A suite of PPE experiments, comprising 128 members, were conducted using the QMC sampling method. Here we first examine the mean precipitation over the tropical Pacific as simulated by the ensemble mean of the 128 PPE members (hereinafter referred to as PPE-mean). Figures 1a and 1e illustrate that the observed mean precipitation over the tropical Pacific is concentrated in the Northern Hemisphere ITCZ, the Southern Hemisphere South Pacific convergence zone (SPCZ) and the eastern Pacific warm pool region. The PPE-mean reproduces the general spatial pattern of the mean precipitation well, such as the southeastward tilting of the SPCZ as observed in the PPE-mean (Figure 1b). However, it tends to overestimate the precipitation intensity across most of the tropical regions characterized by abundant rainfall (Figure 1c). Furthermore, the spread of the difference in the mean precipitation simulations

among the 128 members (Figure 1d) resembles the spatial pattern of mean precipitation, suggesting that the uncertain parameters of interest in this study may be pivotal in determining the mean precipitation simulation over the tropical Pacific. Additionally, a Taylor diagram (Taylor, 2001) is provided in Figure S3a to show the spread of the mean precipitation simulations among 128 PPE members. As indicated by the pattern correlation coefficient (PCC) and the ratio of spatial standard deviations of the simulations against the observation (hereafter SDR), all the PPE members can yield reasonable spatial pattern and intensity to some extent, although there is spread in both PCC and SDR among the 128 PPE members (for more details, refer to supplementary Text S3).

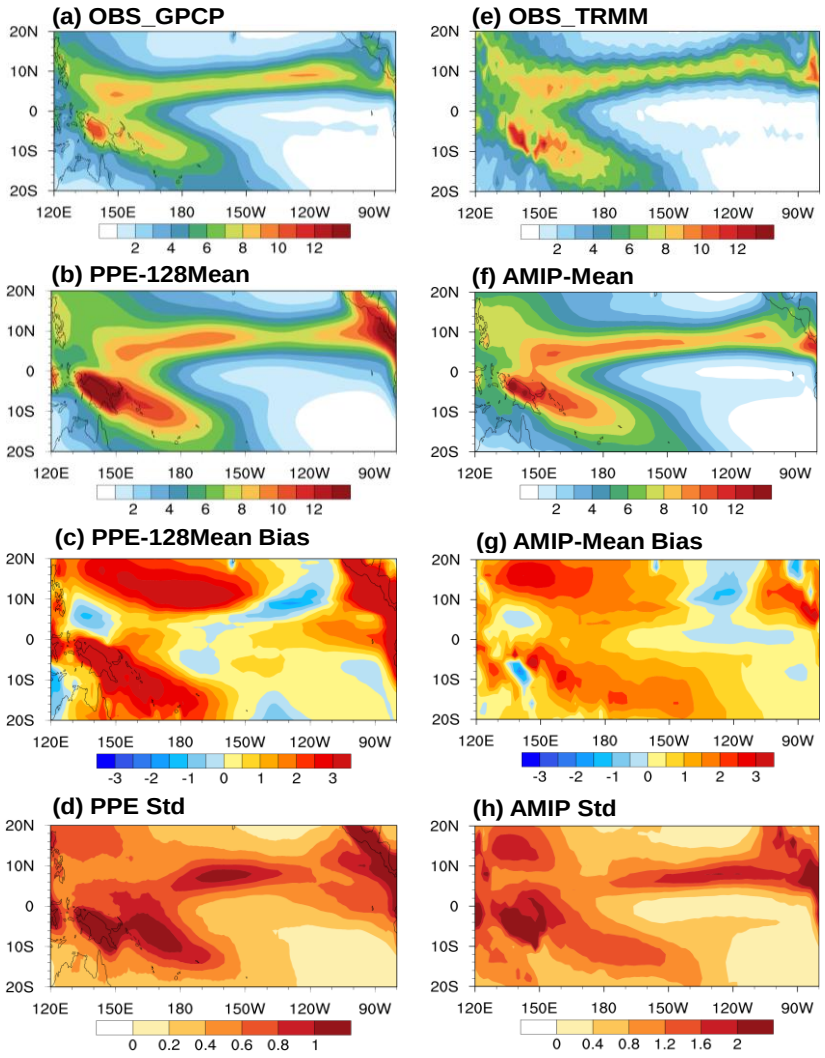

Figure 1. Observed annual mean precipitation from (a) GPCP and (e) TRMM. (b) Annual mean precipitation from PPE multi-member ensemble mean and (c) the bias (PPE-mean minus GPCP). (d) Spread of the PPE members, which is indicated by one standard deviation among PPE multi-members. (f-h) are same as (b-d) but for the AMIP simulations from thirty CMIP6 models. Unit: mm day^{-1}.

We also assessed the performance of the AMIP simulations from thirty CMIP6 models. Figures 1f-h show the multi-model ensemble mean of these AMIP simulations (hereafter AMIP-Mean) (Figure 1f), the biases from AMIP-Mean (Figure 1g), and the spread among these thirty models as quantified by calculating the standard deviation of their simulation biases (Figure 1h). It is found that the spatial pattern of mean precipitation simulation biases from AMIP-mean resemble that from PPE-mean (compare Figure 1c with Figure 1g), with both exhibiting an overestimation of mean precipitation over most of the tropical Pacific. Likewise, the spread of AMIP simulation biases among the 30 CMIP models is analogous to the spread among the 128 PPE members (compare Figure 1d with Figure 1h). These findings suggest that the insights gained from the CAM6 model may offer clues applicable to other AGCMs, as they seem to exhibit similar biases in simulating mean precipitation over the tropical Pacific.

3.2 Sensitivity of Tropical Pacific Precipitation Simulation to the Perturbed Parameters

In each PPE member, all 12 parameters are simultaneously perturbed, hence the differences among the 128 members result from the linear effect and the nonlinear effect due to the interaction among the perturbed parameters. To extract the most significant spatial characteristic of the mean precipitation bias in response to the perturbed parameters, an empirical orthogonal function (EOF) analysis was performed on the 128 members of PPE mean precipitation biases, in which each member is treated as a sample. Figures 2a and 2e show the inter-member EOF modes of PPE mean precipitation biases. The EOF1 mode, which explains 40.2% of the variance, reflects the major difference of mean precipitation biases among these members. It is characterized by a large area of positive anomaly over Maritime Continent, the SPCZ, and the central eastern Pacific, with negative anomaly centered over the waters north of New Guinea and the eastern Pacific warm pool. The EOF2, which explains 16.5% of the variance, is characterized by mean precipitation biases mainly loading over the northern hemisphere ITCZ region and the SPCZ region.

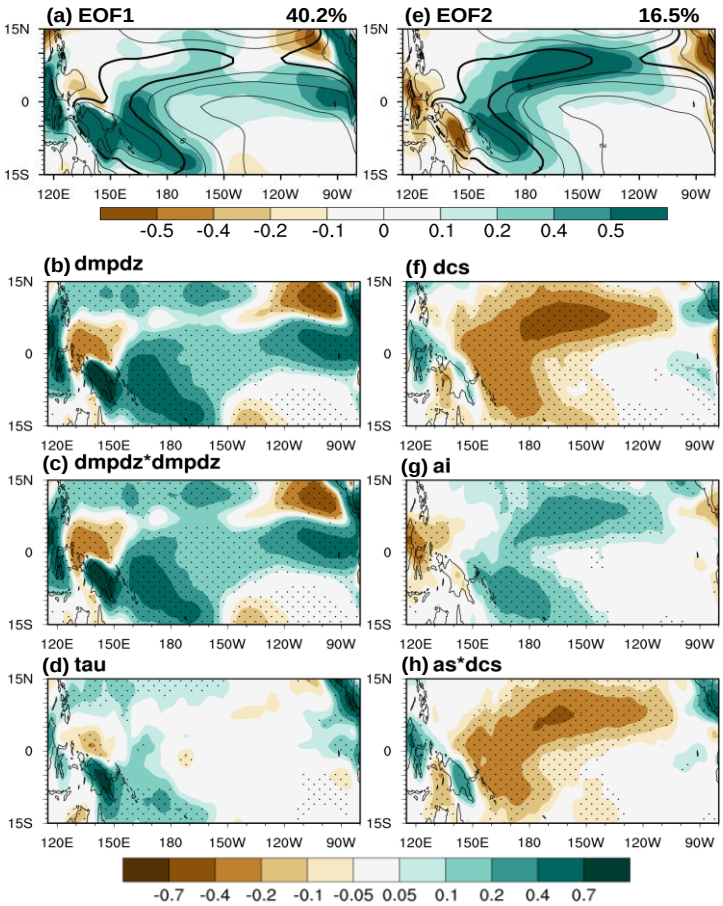

Figure 2. (a, e) The first two EOF modes (shading) of the simulation biases of mean precipitation derived from 128 PPE members, along with the mean precipitation from the PPE multi-member ensemble mean (contours, unit: mm day^{-1}, interval is 2 mm day^{-1}, with bold curve indicating 8 mm day^{-1}). The percentages in the upper right corner represent the explained variances, and these two EOF models are well separated from each other and from other modes based on North criterion (North et al., 1982). (b-d) The regression pattern of mean precipitation simulation biases onto the normalized series of (b) *dmpdz*, (c) *dmpdz*dmpdz*, and (d) *tau* from the 128 PPE members. Dots indicate regions where the regression results exceed the 95% confidence level. Unit: mm day^{-1}. (f-h) same as (b-d) but for the responses to normalized series of *dcs*, *ai*, and *as*dcs*.

To quantitatively analyze the impacts of each parameter on these two leading modes, the GLM method (see Section 2.3.2) was employed. Specifically, the GLM method was directly applied to PC1 and PC2 to calculate the relative contributions of each term to the first two leading modes (for more details, see Text S4). As listed in Table S3, the terms that primarily contribute to the EOF1 mode include the linear impacts of *dmpdz* (fractional rate of entrainment) and *tau* (convective timescale), as well as nonlinear impact of the quadratic term of *dmpdz*. On the other hand, the linear impacts of *dcs* (autoconverion size threshold for ice to snow) and *ai* (fall speed parameter for cloud ice), along with nonlinear term of the interaction between *dcs*

and *as* (fall speed parameter for snow), primarily contribute to the EOF2 mode. Our subsequent analysis will further demonstrate that EOF1 mode is primarily influenced by convective scheme parameters, leading us to designate it as the Convection-Para mode. Similarly, as EOF2 mode is mainly dominated by parameters associated with cloud ice, hence it is termed the CloudIce-Para mode. The physical interpretation behind the parameters' impacts will be explained in Section 3.3.

3.3 Impacts of Key Terms and Related Physical Interpretation

3.3.1 Key Terms Contributing to Convection-Para Mode

The parameter *dmpdz* represents the ratio at which the surrounding air mass is entrained into a convective updraft in a vertical column per km. To further analyze the response of mean precipitation to the perturbation in *dmpdz*, the simulation biases of mean precipitation (simulation minus GPCP) in 128 PPE members were regressed onto the normalized series of *dmpdz* (Figure 2b). It is found that the spatial pattern of the response of mean precipitation biases to the perturbed *dmpdz* (Figure 2b) closely mirrors the EOF1 pattern (Figure 2a). Along with the increase of *dmpdz*, mean precipitation tends to increase across most of the regions studied, but decreases in the areas north of New Guinea and the Eastern Pacific warm pool.

The physical interpretation of the impact of the change in *dmpdz* on the mean precipitation is given below. In deep convection schemes, the initiation of deep convection is contingent upon the attainment of a critical dilute CAPE threshold. When *dmpdz* intensifies, the entrainment becomes strengthened correspondingly. On one hand, enhanced entrainment causes a greater influx of dry air into the cloud, which increases the evaporation of cloud droplets. Consequently, it becomes harder for the formation of convection, inhibiting the convective precipitation (Figure 3a; Emmenegger et al., 2024). On the other hand, the increased strength of entrainment curtails the deep convection, thereby diminishing the convective depletion of water vapor. This, in turn, elevates humidity at the grid scale, resulting in a stronger large-scale precipitation response (Figure 3d; Qian et al., 2015). Given that total precipitation (PrecT) in the model simulation is the sum of convective precipitation (PrecC) and large-scale precipitation (PrecL), the mean precipitation response to changes in *dmpdz* (Figure 2b) is a consequence of alterations in both mean PrecC (Figure 3a) and mean PrecL (Figure 3d). This

conclusion is further confirmed by the single-parameter perturbation experiments, in which *dmpdz* is the sole parameter altered while all other parameters maintained at their default settings. As depicted in Figure S4, along with the increase of *dmpdz*, PrecC diminishes while PrecL intensifies. In this sense, there appears to be a competitive dynamic between PrecC and PrecL in response to the altered *dmpdz*, with the overall changes in PrecT hinging on the comparative magnitude of the changes from each component. As *dmpdz* increases, the enhancement in PrecL surpasses the reduction in PrecC across most of the tropical Pacific, except for two relatively small regions (north of the New Guinea and the eastern Pacific warm pool). This results in an overall increase in mean PrecT across most of the tropical Pacific but a decrease in mean PrecT in the area north of the New Guinea and the eastern Pacific warm pool in response to the altered *dmpdz*, as illustrated in Figure 2b.

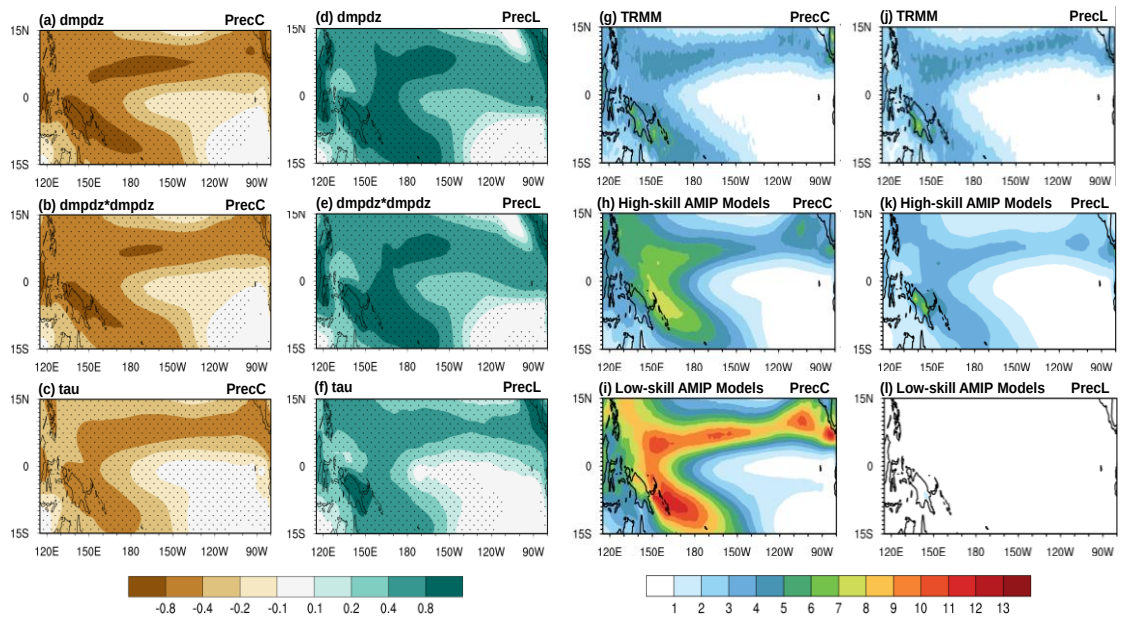

Figure 3. (a-c) The regression pattern of mean PrecC onto the normalized series of (a) *dmpdz*, (b) *dmpdz*dmpdz*, and (c) *tau* from the 128 PPE members. Dots indicate regions where the regression results exceed the 95% confidence level. Unit: mm day^{-1}. (d-f) same as (a-c), but for the mean PrecL. (g-i) Mean PrecC (mm day^{-1}) from (g) TRMM, (h) high-skill AMIP models and (i) low-skill AMIP models. In the context, using TRMM-based PrecC/PrecT ratio as a rough reference, five models with relatively high-skill in representing the PrecC/PrecT ratio (as denoted by the numbers 29, 7, 15, 17, and 5 in Figure S6) are grouped into high-skill AMIP models; and another five models with relatively low-skill in representing the PrecC/PrecT ratio (as indicated by the numbers 31, 24, 3, 28, and 27 in Figure S6) are grouped into low-skill AMIP models. (j-l) same as (g-i), but for the mean PrecL.

It is noteworthy that nonlinear term *dmpdz*dmpdz* also contributes to the PrecT (Table S3). In fact, when other parameters are held default and only *dmpdz* is perturbed (Figure S4), the

results show that when *dmpdz* is less than 0.375 km^{-1}, the reduction in mean PrecC dominates, and the PrecT decreases as *dmpdz* increases; when *dmpdz* is greater than 0.375 km^{-1}, the increase in PrecL dominates, and the PrecT increases as *dmpdz* increasing. The inflection point within the monotonic trend (Figure S4a) suggests that the overall mean PrecT demonstrates a pattern of change proportional to the square of *dmpdz*. This indicates that the nonlinear term *dmpdz*dmpdz* also contributes to the mean PrecT.

Tau (convective timescale) represents the characteristic time scale with which CAPE is depleted at an exponential rate by convection. The response pattern of mean PrecT to *tau* aligns with that of EOF1. Specifically, as *tau* increases, mean PrecT tends to increase across most of the tropical Pacific but decrease in the region north of New Guinea and the eastern Pacific warm pool (Figure 2d). Analogous to the effects of *dmpdz*, changes in *tau* also yield contrasting trends in mean PrecC and mean PrecL (Figures 3c and 3f). Given a constant level of CAPE, which signifies the energy available for atmospheric convection (Moncrieff & Miller, 1976), an increase in *tau* leads to a deceleration in CAPE consumption. Consequently, the air parcel acquires kinetic energy at a reduced rate, leading to suppressed deep convection. This results in an increase in atmospheric humidity and a subsequent intensification of PrecL (Mishra & Srinivasan, 2010). Hence, variations in PrecT are also contingent on the relative extent of changes in local PrecC and PrecL characteristics. This conclusion is further confirmed by the single-parameter perturbation experiments, in which only *tau* is perturbed (Figure S5). It is noteworthy that land precipitation is more sensitive to changes in *tau* compared to the precipitation over ocean, which may be related to the greater sensitivity of land precipitation diurnal cycle to *tau* (Qian et al., 2015).

The above analysis elucidates how the key terms that stem from the convection parameterization influence the ratio of PrecC to PrecT (hereafter PrecC/PrecT ratio) and ultimately affect the simulation of mean PrecT in CAM6. We now zoom out to examine the relationship between the PrecC/PrecT ratio and mean precipitation across the AMIP models. The TRMM dataset shows that mean PrecC (Figure 3g) and mean PrecL (Figure 3j) are approximately equal. Although the TRMM-based PrecC/PrecT ratio is used as a rough reference, all thirty AMIP simulations overestimate the PrecC/PrecT ratio (x-axis in Figure S6)

to various extent. As denoted by the numbers 29, 7, 15, 17, and 5 in Figure S6, these five models, which possess the lowest PrecC/PrecT ratios, show the greatest alignment with the reference point from TRMM observation, and hence they are referred to as the high-skill AMIP models in terms of accurately replicating the PrecC/PrecT ratio. Besides, another five models with the highest PrecC/PrecT ratios, as indicated by the numbers 31, 24, 3, 28, and 27, show a PrecC/PrecT ratio nearly twice the reference value from TRMM, and thus they are grouped into the low-skill AMIP models. It is noted that a more accurate representation of PrecC/PrecT ratio tends to correspond to a more realistic simulation of PrecT (Figure S6). The composite results based on five models with relatively high-skill in depicting the PrecC/PrecT ratio show that mean PrecC (Figure 3h) is slightly larger than mean PrecL (Figure 3k); while in the models with relatively low-skill in representing the PrecC/PrecT ratio, mean PrecC (Figure 3i) is much larger than mean PrecL (Figure 3l). As shown in Figure S7, the difference in mean PrecT between high-skill and low-skill models is characterized by overestimated mean PrecT over most of the equatorial Pacific, exhibiting a pattern correlation coefficient of 0.43 with EOF1. This indicates that not only in CAM6 but also in other AGCMs, the convective parameters likely play a critical role in inducing the bias in the PrecC/PrecT ratio, which in turn affects the biases in mean PrecT.

3.3.2 Key Terms Contributing to CloudIce-Para Mode

In addition to the GLM analysis that demonstrates that two linear terms (*dcs* and *ai*) and one nonlinear term (*as*dcs*) are responsible for the CloudIce-Para mode (EOF2), Figures 2f-h further illustrate that the response patterns of the mean precipitation simulation biases to the linear terms of *dcs* (autoconversion size threshold for ice to snow) and *ai* (fall speed parameter for cloud ice) as well as the nonlinear term *as*dcs* (interaction term between *as* and *dcs*), closely resemble the pattern of EOF2.

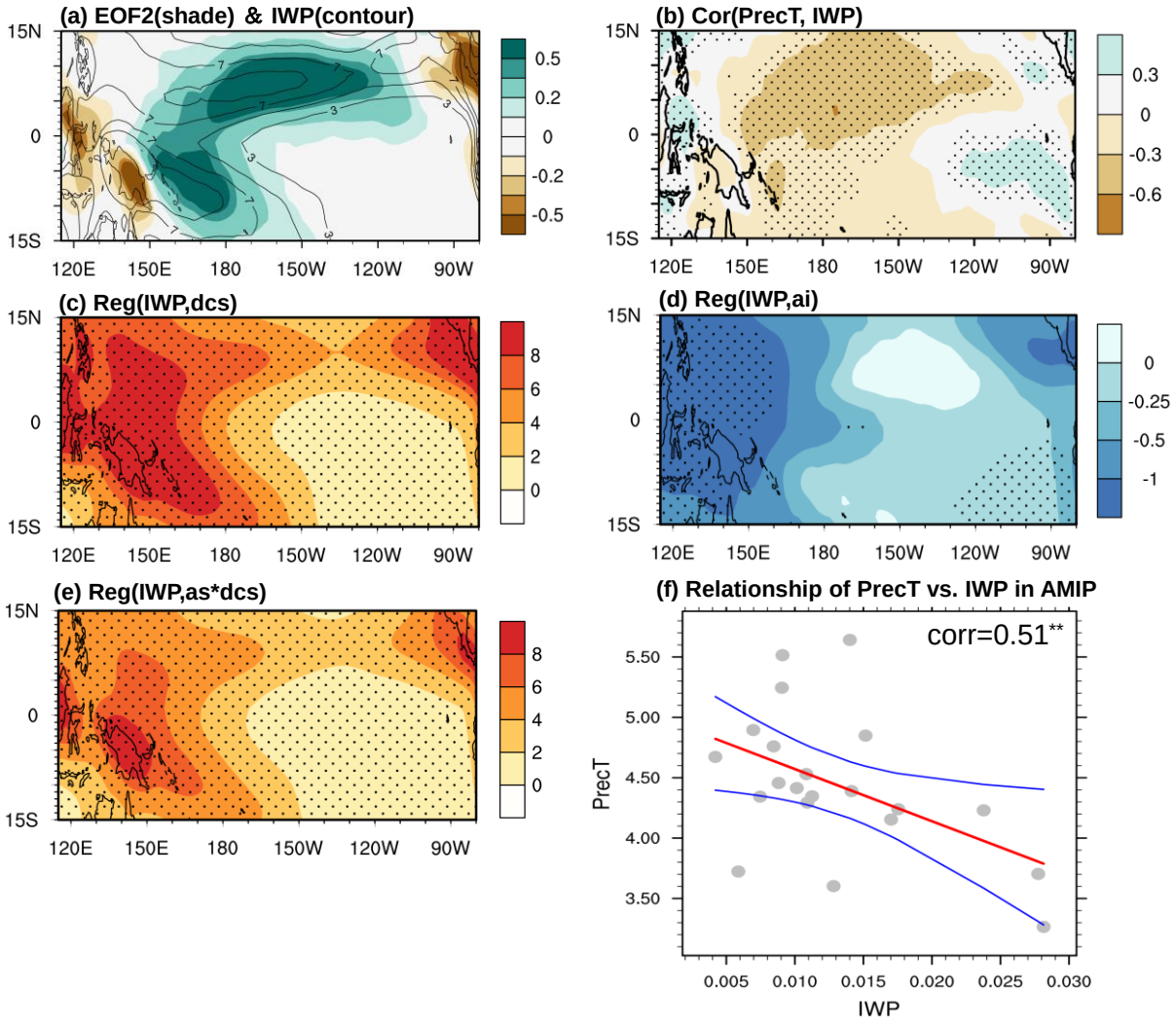

Figure 4. (a) EOF2 mode (shading) overlaid by mean IWP (contour intervals are 3, 5, 7, 9*10^{-3} kg m^{-2}) derived from the PPE experiments. (b) Correlation map between mean precipitation and mean IWP in-situ among the 128 PPE members, which is obtained by calculating the correlation coefficients between mean precipitation at a certain grid and the corresponding mean IWP at that grid based on 128 PPE members. (c-e) The regression pattern of mean IWP onto the normalized series of (c) *dcs*, (d) *ai*, and (e) *as*dcs* from 128 PPE members (10^{-3} kg m^{-2}). The dots in (b-e) indicating regions where the correlation or regression results exceed the 95% confidence level. (f) Scatter diagram showing the relationship between mean IWP and mean precipitation in the main ITCZ region (0–10°N, 180–220°E) from AMIP models. Red line represents the best linear fit and blue lines denote the 95% confidence range of the linear regression. The correlation coefficient equals to 0.51, exceeding the 95% confidence level.

It is acknowledged that cloud microphysics parameters, such as *dcs* and *ai*, can influence the ice water path (IWP) (Zhao et al., 2013; Eidhammer et al. 2014; Pathak et al., 2020) and the associated large-scale precipitation (Sanderson et al., 2008; Qian et al., 2015), thereby affecting the total precipitation. Figure S8 confirms that the response of the simulated PrecT to the adjustments of *dcs*, *ai*, and *as*dcs* (left columns in Fig. S8) is primarily attributed to the changes

in the simulated PrecL to these adjustments (right columns in Fig. S8), while the contributions of the PrecC changes are relatively minor (middle columns in Fig. S8). Hence, we present only the results for PrecT in the following analysis.

As shown in Figure 4a, compared to clouds over land, deep convective clouds with ice tops over the ITCZ region exhibit a substantial amount of mean IWP, aligning with the findings of Tubul et al. (2017). In the ITCZ region, mean IWP tends to be inversely correlated with mean precipitation in the PPE results (Figure 4b). Indeed, such a relationship is also observed in the AMIP models, i.e., mean IWP is negatively correlated with mean precipitation over the main ITCZ region (Figure 4f). This indicates that mean precipitation over the main ITCZ region is closely associated with mean IWP, both of which can be traced back to the cloud microphysics parameters associated with cloud ice.

The influence of *dcs* (autoconversion size threshold for ice to snow) on mean IWP (Figure 4c) and the relevant mean precipitation is interpreted firstly. Within the model, cloud ice suspended in the air must reach a certain size to acquire sufficient gravity to overcome buoyancy and thereby fall as snow, which eventually melts to contribute to rainfall. Therefore, as the parameter *dcs* increases, cloud ice must grow larger to convert to snow, leading to an increase in the IWP (Figure 4c) but a decrease in both snowfall and rainfall (Figure 2f); and vice versa. In terms of the influence of *ai* (fall speed of cloud ice), an increase in *ai* accelerates the descent of ice particles and hence enhances the collision and growth of ice nuclei, which speeds up the formation of precipitation and improves the conversion efficiency of cloud ice into precipitation. This accounts for the decrease in mean IWP (Figure 4d) and the increase in the mean precipitation (Figure 2g) in response to the increase of *ai*.

It is intriguing to note that the nonlinear effect of *as*dcs* (where "*as*" is the fall speed parameter for snow) exerts a pronounced effect on mean IWP (Figure 4e) and mean precipitation (Figure 2h), whereas the linear effect of *as* on mean IWP and mean precipitation is insignificant (not shown). As indicated by Loftus and Wordsworth (2021), the drag force exerted by precipitation particles on the air can be expressed as:

$$F_{drag} = \frac{1}{2} C_D A \rho_{air} v^2 \quad (2)$$

where C_D is the drag coefficient, A is the cross-sectional area of the particle, ρ_{air} is the air

density, and v is the particle's falling speed relative to air. Therefore, when both *dcs* is large and *as* is large (with the former indicating a larger cross-sectional area of the particle, A, and the latter indicating a greater particle falling speed, v), the drag force is large, leading to powerful downdraft air current that impedes precipitation; and the opposite effect is observed when both *dcs* and *as* are small. This elucidates the mechanism by which the interplay between *dcs* and *as* influences the precipitation within the simulation.

The above analysis explains how the key terms associated with cloud ice influence mean IWP and ultimately affect mean precipitation in CAM6. It is noteworthy that the relationship between mean IWP and mean precipitation over the main ITCZ region among the AMIP models is consistent with the PPE results. This indicates that despite the use of varying parameterization schemes across AGCMs, the influence of the cloud ice-related parameters on mean precipitation simulations warrants more consideration.

4. Summary

In this study, we conducted a suite of PPE experiments to investigate the influence of the key parameters within the deep convection scheme and the cloud physics scheme of the CAM6 model on simulating mean precipitation in the tropical Pacific. Firstly, twelve selected parameters from deep convection and cloud physics schemes were simultaneously perturbed based on the QMC sampling approach; and then the PPE experiments that have 128 members and cover the period of 1979-2014 were obtained. Through conducting the EOF analysis and the GLM analysis, we identified the critical parameters those have the most influential effects on the tropical Pacific precipitation simulations, and found that the parameters' effects can be clearly separated into two distinct categories: those primarily governed by the convection scheme, which reflect the competition between PrecC and PrecL, and those predominantly influenced by cloud ice processes. Furthermore, we revealed that the nonlinear effects of these perturbed parameters on the simulation of mean precipitation are significant and warrant careful consideration when tuning multi-parameters synchronously. The interpretation for the impacts of the critical parameters on the mean precipitation simulation is also provided. Besides, some aspects about the biases in simulating mean precipitation in PPE experiments align with those revealed by the AMIP simulations, offering implications for the AGCMs' development.

Specifically, through performing EOF analysis on the mean precipitation biases derived from 128 members of PPE, we extracted the first two leading modes of precipitation response to the adjustment of twelve selected parameters. The GLM analysis reveals that the EOF1 mode is primarily influenced by convection scheme parameters, including the linear impacts of *dmpdz* and *tau*, as well as nonlinear impact of the quadratic term of *dmpdz*. Thus EOF1 is called the Convection-Para mode. Parallelly, the EOF2 mode is largely dominated by parameters associated with cloud ice, encompassing the linear impacts of *dcs* and *ai*, along with nonlinear interaction between *dcs* and *a*. Hence EOF2 is termed the CloudIce-Para mode.

For the Convection-Para mode, the changes in the key convection parameters can induce competition between PrecC and PrecL, which ultimately affect mean PrecT. It is noteworthy that a more accurate representation of PrecC/PrecT ratio tends to correspond to a more realistic simulation of PrecT in the AMIP simulations, indicating the potential importance of the PrecC/PrecT ratio on the simulation of mean PrecT when tuning convection parameters. For the CloudIce-Para mode, the major contributing terms primarily influence mean precipitation by affecting the cloud ice processes and the associated large-scale precipitation. Additionally, the relationship between mean IWP and mean precipitation over the main ITCZ region among the AMIP models is consistent with the PPE results, indicating that despite the use of varying parameterization schemes across AGCMs, the influence of the cloud ice-related parameters on mean precipitation simulations merits more consideration.

Our single-parameter perturbation experiments further elucidate why the nonlinear term of *dmpdz*dmpdz* plays a role in affecting mean precipitation simulation within the CAM6 model. Also, how the interplay between *dcs* and *as* influences the mean precipitation simulation is interpreted. The identified key parameters associated with the convective and cloud microphysics parameterization schemes can be informative for the development of the CESM family and also provide some reference information for the advancement of other AGCMs.

Acknowledgements

We thank three anonymous reviewers for insightful suggestions and comments. This work was jointly supported by the National Key Research and Development Program of China (Grant

2022YFF0802004), NSFC (No. 42005020, 42250710154), and Excellent Youth Natural Science Foundation of Jiangsu Province (BK20230061).

Open Research

Data Availability Statement

The HadISST data is available at Hadley Centre for Climate Prediction and Research (2000). GPCP data is available at Adler et al. (2020). TRMM data is available at Tropical rainfall measurement mission (2011). Model outputs of CMIP6 are obtained at https://esgf-node.llnl.gov/search/cmip6/, and can also be accessed in Eyring et al. (2016).

References

Adler, R. F., Huffman, G. J., Chang, A., Ferraro, R., Xie, P. P., Janowiak, J., et al. (2003). The version-2 global precipitation climatology project (GPCP) monthly precipitation analysis (1979–present). *Journal of hydrometeorology*, *4*(6), 1147-1167.

Adler, R., et al. (2020), updated monthly. Global Precipitation Climatology Project (GPCP) Climate Data Record (CDR), Version 2.3 (Monthly). Research Data Archive at the National Center for Atmospheric Research, Computational and Information Systems Laboratory. [Dataset]. https://doi.org/10.5065/MM6J-9282.

Allan, R. P., Soden, B. J., John, V. O., Ingram, W., & Good, P. (2010). Current changes in tropical precipitation. *Environmental Research Letters*, *5*(2), 025205.

Arakawa, A. (2004). The cumulus parameterization problem: Past, present, and future. *Journal of Climate*, *17*(13), 2493-2525.

Awaka, J., Iguchi, T., & Okamoto, K. I. (2007). Rain type classification algorithm. In *Measuring precipitation from space: EURAINSAT and the future* (pp. 213-224). Dordrecht: Springer Netherlands.

Awaka, J., Iguchi, T., Kumagai, H., & Okamoto, K. I. (1997, August). Rain type classification algorithm for TRMM precipitation radar. In *IGARSS'97. 1997 IEEE international geoscience and remote sensing symposium proceedings. remote sensing-a scientific vision for sustainable development* (Vol. 4, pp. 1633-1635). IEEE.

Bacmeister, J. T., Wehner, M. F., Neale, R. B., Gettelman, A., Hannay, C., Lauritzen, P. H.et al. (2014). Exploratory high-resolution climate simulations using the Community Atmosphere Model (CAM). *Journal of Climate*, *27*(9), 3073-3099.

Burnet, F., & Brenguier, J. L. (2007). Observational study of the entrainment-mixing process in warm convective clouds. *Journal of the Atmospheric Sciences*, *64*(6), 1995-2011.

Caflisch, R. E. (1998). Monte carlo and quasi-monte carlo methods. *Acta numerica*, *7*, 1-49.

Chen, D., & Dai, A. (2019). Precipitation characteristics in the Community Atmosphere Model and their dependence on model physics and resolution. *Journal of Advances in Modeling Earth Systems*, *11*(7), 2352-2374.

Chen, D., Dai, A., & Hall, A. (2021). The convective-to-total precipitation ratio and the "drizzling" bias in climate models. *Journal of Geophysical Research: Atmospheres,*

126(16), e2020JD034198.

Chen, L., Yu, Y., & Sun, D. Z. (2013). Cloud and water vapor feedbacks to the El Niño warming: are they still biased in CMIP5 models?. *Journal of Climate*, *26*(14), 4947-4961.

Chen, L., Sun, D.-Z., Wang, L., & Li, T. (2019), A Further Study on the Simulation of Cloud-Radiative Feedbacks in the ENSO Cycle in the Tropical Pacific with a Focus on the Asymmetry. *Asia-Pacific Journal of Atmospheric Sciences*, 55(3), 303-316.

Dai, A. (2006). Precipitation characteristics in eighteen coupled climate models. *Journal of climate*, *19*(18), 4605-4630.

Danabasoglu, G., Lamarque, J. F., Bacmeister, J., Bailey, D. A., DuVivier, A. K., Edwards, J., et al. (2020). The community earth system model version 2 (CESM2). *Journal of Advances in Modeling Earth Systems*, *12*(2), e2019MS001916.

Donner, L. J., Seman, C. J., Hemler, R. S., & Fan, S. (2001). A cumulus parameterization including mass fluxes, convective vertical velocities, and mesoscale effects: Thermodynamic and hydrological aspects in a general circulation model. *Journal of climate*, *14*(16), 3444-3463.

Duffy, M. L., Medeiros, B., Gettelman, A., & Eidhammer, T. (2024). Perturbing parameters to understand cloud contributions to climate change. *Journal of Climate, 37*, 213–227.

Eidhammer, T., Gettelman, A., Thayer-Calder, K., Watson-Parris, D., Elsaesser, G., Morrison, H., et al. (2024). An extensible perturbed parameter ensemble for the community atmosphere model version 6. *Geosci. Model Dev.*, 17, 7835-7853.

Eidhammer, T., Morrison, H., Bansemer, A., Gettelman, A., & Heymsfield, A. J. (2014). Comparison of ice cloud properties simulated by the Community Atmosphere Model (CAM5) with in-situ observations. *Atmospheric Chemistry and Physics*, *14*(18), 10103-10118.

Emmenegger, T., Ahmed, F., Kuo, Y., Xie, S., Zhang, C., Tao, C., et al., (2024). The Physics behind Precipitation Onset Bias in CMIP6 Models: The Pseudo-Entrainment Diagnostic and Trade-Offs between Lapse Rate and Humidity. *Journal of Climate, 37*(6), 2013-2033.

Eyring, V., Bony, S., Meehl, G. A., Senior, C. A., Stevens, B., Stouffer, R. J., & Taylor, K. E. (2016). Overview of the Coupled Model Intercomparison Project Phase 6 (CMIP6)

experimental design and organization. *Geoscientific Model Development*, *9*(5), 1937-1958.

Eyring, V., Bony, S., Meehl, G., Senior, C., Stevens, B., Stouffer, R., & Taylor, K. (2016). Overview of the Coupled Model Intercomparison Project Phase 6 (CMIP6) experimental design and organization [Dataset]. Geoscientific Model Development, 9(5), 1937–1958. https://doi.org/10.5194/gmd-9-1937-2016.

Fiedler, S., Crueger, T., D'Agostino, R., Peters, K., Becker, T., Leutwyler, D., et al. (2020). Simulated tropical precipitation assessed across three major phases of the coupled model intercomparison project (CMIP). *Monthly Weather Review*, *148*(9), 3653-3680.

Fläschner, D., Mauritsen, T., & Stevens, B. (2016). Understanding the intermodel spread in global-mean hydrological sensitivity. *Journal of Climate*, *29*(2), 801-817.

Fowler, L. D., Randall, D. A., & Rutledge, S. A. (1996). Liquid and Ice Cloud Microphysics in the CSU General Circulation Model. Part 1: Model Description and Simulated Microphysical Processes. *Journal of Climate, 9*(3), 489-529.

Ge, Z.-A., & Chen, L. (2020). Preliminary analysis of the zonal distribution of ENSO-related SSTA in three CMIP5 coupled models. *Atmospheric and Oceanic Science Letters*, 13(5), 443-451.

Gettelman, A., & Morrison, H. (2015). Advanced two-moment bulk microphysics for global models. Part I: Off-line tests and comparison with other schemes. *Journal of Climate, 28*(3), 1268-1287.

Gettelman, A., Eidhammer, T., Duffy, M. L., McCoy, D. T., Song, C., & Watson-Parris, D. (2024). The interaction between climate forcing and feedbacks. Journal of Geophysical Research: Atmospheres, 129(18), e2024JD040857.

Guo, Z., Wang, M., Qian, Y., Larson, V. E., Ghan, S., Ovchinnikov, M., et al. (2014). A sensitivity analysis of cloud properties to CLUBB parameters in the single-column Community Atmosphere Model (SCAM5). *Journal of Advances in Modeling Earth Systems, 6*(3), 829-858.

Hadley Centre for Climate Prediction and Research/Met Office/Ministry of Defence/United Kingdom. (2000), updated monthly. Hadley Centre Global Sea Ice and Sea Surface Temperature (HadISST). Research Data Archive at the National Center for Atmospheric

561 Research, Computational and Information Systems Laboratory. [Dataset].
562 https://doi.org/10.5065/XMYE-AN84.
563 He, L., Zhou, T., & Chen, X. (2023). South Asian summer rainfall from CMIP3 to CMIP6
564 models: Biases and improvements. *Climate Dynamics, 61*(3), 1049–1061.
565 Held, I. M., Zhao, M., & Wyman, B. (2007). Dynamic radiative–convective equilibria using
566 GCM column physics. *Journal of the atmospheric sciences, 64*(1), 228-238.
567 Her, Y., Yoo, S. H., Cho, J., Hwang, S., Jeong, J., & Seong, C. (2019). Uncertainty in
568 hydrological analysis of climate change: multi-parameter vs. multi-GCM ensemble
569 predictions. *Scientific reports*, *9*(1), 4974.
570 Hou, Z., Huang, M., Leung, L. R., Lin, G., & Ricciuto, D. M. (2012). Sensitivity of surface flux
571 simulations to hydrologic parameters based on an uncertainty quantification framework
572 applied to the Community Land Model. *Journal of Geophysical Research: Atmospheres*,
573 *117*(D15).
574 Jinfang, Y., Donghai, W., Huangbin, X., Guoqing, Z., & Xiaoling, J. (2015). A Study of the
575 Effects of Ice Nuclei on Cloud Microphysical Properties and Precipitation. *Advances in*
576 *Earth Science*, *30*(3), 323.
577 Kirtman, B. P., Fan, Y., & Schneider, E. K. (2002). The COLA global coupled and anomaly
578 coupled ocean–atmosphere GCM. *Journal of climate, 15*(17), 2301-2320.
579 Kozu, T., Kawanishi, T., Kuroiwa, H., Kojima, M., Oikawa, K., Kumagai, H., Nishikawa, K.,
580 et al. (2001). Development of precipitation radar onboard the Tropical Rainfall Measuring
581 Mission (TRMM) satellite. *IEEE transactions on geoscience and remote sensing, 39*(1),
582 102-116.
583 Li, G., & Xie, S. (2014). Tropical Biases in CMIP5 Multimodel Ensemble: The Excessive
584 Equatorial Pacific Cold Tongue and Double ITCZ Problems. *Journal of Climate, 27*(4),
585 1765-1780.
586 Li, G., & Xie, S. P. (2012). Origins of tropical-wide SST biases in CMIP multi-model
587 ensembles. *Geophysical research letters, 39*(22).
588 Li, H., Huang, M., Wigmosta, M. S., Ke, Y., Coleman, A. M., Leung, L. R., et al. (2011).
589 Evaluating runoff simulations from the Community Land Model 4.0 using observations

590 from flux towers and a mountainous watershed. *Journal of Geophysical Research:*
591 *Atmospheres*, *116*(D24).
592 Li, L., Wang, B., & Zhang, G. J. (2014). The role of convective condensation processes in
593 response of surface shortwave cloud radiative forcing to El Niño warming. *Journal of*
594 *Climate*, 27(17), 6721-6736.
595 Li, L., Wang, B., Dong, L. et al. (2013) Evaluation of grid-point atmospheric model of IAP
596 LASG version 2 (GAMIL2). *Advances in Atmospheric Sciences*, 30, 855–867.
597 Lin, J. (2007). The Double-ITCZ Problem in IPCC AR4 Coupled GCMs: Ocean–Atmosphere
598 Feedback Analysis. *Journal of Climate*, *20*(18), 4497-4525.
599 Liu, X., & Grise, K. M. (2023). Implications of warm pool bias in CMIP6 models on the
600 Northern Hemisphere wintertime subtropical jet and precipitation. *Geophysical Research*
601 *Letters*, *50*(15), e2023GL104896.
602 Loftus, K., & Wordsworth, R. D. (2021). The physics of falling raindrops in diverse planetary
603 atmospheres. *Journal of Geophysical Research: Planets*, *126*(4), e2020JE006653.
604 Ma, L., & Jiang, Z. (2020). Improved leading modes of interannual variability of the Asian-
605 Australian monsoon in an AGCM via incorporating a stochastic multicloud model.
606 *Climate Dynamics*, 54(1), 759-775.
607 Ma, L., & Yang, S. (2020). Impacts of the stochastic multicloud parameterization on the
608 simulation of Western North Pacific summer rainfall. *Atmospheric Research*, 244, 105067.
609 Manabe, S., Smagorinsky, J., & Strickler, R. F. (1965). Simulated climatology of a general
610 circulation model with a hydrological cycle. *Monthly Weather Review*, *93*(12), 769-798.
611 Mechoso, C. R., Robertson, A. W., Barth, N., Davey, M. K., Delecluse, P., Gent, P. R., et al.
612 (1995). The seasonal cycle over the tropical Pacific in coupled ocean–atmosphere general
613 circulation models. *Monthly Weather Review*, *123*(9), 2825-2838.
614 Meehl, G. A., Stocker, T., Collins, W. D., Friedlingstein, P., Gaye, A. T., Gregory, J. M., et al.
615 (2007). Global climate projections. In Climate Change 2007: The physical science basis.
616 Contribution of Working Group I to the Fourth Assessment Report of the
617 Intergovernmental Panel on Climate Change, Cambridge Univ. Press, Cambridge, U. K.
618 Mishra, S. K., & Srinivasan, J. (2010). Sensitivity of the simulated precipitation to changes in

convective relaxation time scale. In *Annales Geophysicae* (Vol. 28, No. 10, pp. 1827-1846). Göttingen, Germany: Copernicus Publications.

Moncrieff, M. W., & Miller, M. J. (1976). The dynamics and simulation of tropical cumulonimbus and squall lines. *Quarterly Journal of the Royal Meteorological Society*, *102*(432), 373-394.

Morrison, H., & Gettelman, A. (2008). A new two-moment bulk stratiform cloud microphysics scheme in the Community Atmosphere Model, version 3 (CAM3). Part I: Description and numerical tests. *Journal of Climate*, *21*(15), 3642-3659.

Murphy, J. M., Sexton, D. M., Barnett, D. N., Jones, G. S., Webb, M. J., Collins, M., & Stainforth, D. A. (2004). Quantification of modelling uncertainties in a large ensemble of climate change simulations. *Nature*, *430*(7001), 768-772.

Neale, R. B., Richter, J. H., & Jochum, M. (2008). The impact of convection on ENSO: From a delayed oscillator to a series of events. *Journal of climate*, *21*(22), 5904-5924.

North, G. R., Bell, T. L., Cahalan, R. F., & Moeng, F. J. (1982). Sampling errors in the estimation of empirical orthogonal functions. *Monthly weather review*, *110*(7), 699-706.

Oort, A. H., & Peixóto, J. P. (1983). Global angular momentum and energy balance requirements from observations. *Advances in geophysics* (Vol. 25, pp. 355-490). Elsevier.

Pendergrass, A. G., & Hartmann, D. L. (2014). Changes in the distribution of rain frequency and intensity in response to global warming. *Journal of Climate*, *27*(22), 8372-8383.

Qian, Y., Yan, H., Hou, Z., Johannesson, G., Klein, S., Lucas, D., et al. (2015). Parametric sensitivity analysis of precipitation at global and local scales in the Community Atmosphere Model CAM5. *Journal of Advances in Modeling Earth Systems*, *7*(2), 382-411.

Rayner, N. A. A., Parker, D. E., Horton, E. B., Folland, C. K., Alexander, L. V., Rowell, D. P., et al. (2003). Global analyses of sea surface temperature, sea ice, and night marine air temperature since the late nineteenth century. *Journal of Geophysical Research: Atmospheres*, *108*(D14).

Richter, J. H., & Rasch, P. J. (2008). Effects of convective momentum transport on the atmospheric circulation in the Community Atmosphere Model, version 3. *Journal of*

Climate, *21*(7), 1487-1499.

Sanderson, B. M., Piani, C., Ingram, W. J., Stone, D. A., & Allen, M. R. (2008). Towards constraining climate sensitivity by linear analysis of feedback patterns in thousands of perturbed-physics GCM simulations. *Climate Dynamics*, *30*, 175-190.

Schiro, K. A., Su, H., Wang, Y., Langenbrunner, B., Jiang, J. H., & Neelin, J. D. (2019). Relationships between tropical ascent and high cloud fraction changes with warming revealed by perturbation physics experiments in CAM5. *Geophysical Research Letters*, *46*(16), 10112-10121.

Sobol', I. Y. M. (1967). On the distribution of points in a cube and the approximate evaluation of integrals. *Zhurnal Vychislitel'noi Matematiki i Matematicheskoi Fiziki*, *7*(4), 784-802.

Song, X., & Zhang, G. J. (2009). Convection parameterization, tropical Pacific double ITCZ, and upper-ocean biases in the NCAR CCSM3. Part I: Climatology and atmospheric feedback. *Journal of Climate*, *22*(16), 4299-4315.

Stephens, G. L., L'Ecuyer, T., Forbes, R., Gettelmen, A., Golaz, J. C., Bodas-Salcedo, A., et al. (2010). Dreary state of precipitation in global models. *Journal of Geophysical Research: Atmospheres*, *115*(D24).

Stouffer, R. J., Eyring, V., Meehl, G. A., Bony, S., Senior, C., Stevens, B., & Taylor, K. E. (2017). CMIP5 scientific gaps and recommendations for CMIP6. *Bulletin of the American Meteorological Society*, 98(1), 95-105.

Sundqvist, H., Berge, E., & Kristjánsson, J. E. (1989). Condensation and cloud parameterization studies with a mesoscale numerical weather prediction model.

Supharatid, S., Aribarg, T., & Nafung, J. (2022). Bias-corrected CMIP6 climate model projection over Southeast Asia. *Theoretical and Applied Climatology*, *147*, 669-690.

Taylor, K. E. (2001). Summarizing multiple aspects of model performance in a single diagram. *Journal of geophysical research: atmospheres*, *106*(D7), 7183-7192.

Tian, B. (2015). Spread of model climate sensitivity linked to double-Intertropical Convergence Zone bias. *Geophysical Research Letters*, 42(10), 4133-4141.

Trenberth, K. E. (2011). Changes in precipitation with climate change. *Climate research*, *47*(1-2), 123-138.

Tropical Rainfall Measuring Mission (TRMM). (2011), TRMM Radar Rainfall Statistics L3 1 month (5 x 5) and (0.5 x 0.5) degree V7, Greenbelt, MD, Goddard Earth Sciences Data and Information Services Center (GES DISC). [Dataset]. https://disc.gsfc.nasa.gov/datacollection/TRMM_3A25_7.html.

Tubul, Y., Koren, I., Altaratz, O., & Heiblum, R. H. (2017). On the link between precipitation and the ice water path over tropical and mid-latitude regimes as derived from satellite observations. *Atmospheric Measurement Techniques Discussions*, 2017, 1-16.

Wang, B., Wu, R., & Fu, X. (2000). Pacific–East Asian teleconnection: how does ENSO affect East Asian climate?. *Journal of climate*, *13*(9), 1517-1536.

Wang, C., Qian, Y., Duan, Q., Huang, M., Berg, L. K., Shin, H. H., et al. (2020). Assessing the sensitivity of land-atmosphere coupling strength to boundary and surface layer parameters in the WRF model over Amazon. *Atmospheric Research*, *234*, 104738.

Wang, C., Zhang, L., Lee, S. K., Wu, L., & Mechoso, C. R. (2014). A global perspective on CMIP5 climate model biases. *Nature Climate Change*, *4*(3), 201-205.

Wang, W., Chakraborty, T. C., Xiao, W., & Lee, X. (2021). Ocean surface energy balance allows a constraint on the sensitivity of precipitation to global warming. *Nature Communications*, *12*(1), 2115.

Wang, X., & Sloan, I. H. (2008). Low discrepancy sequences in high dimensions: How well are their projections distributed? *Journal of Computational and Applied Mathematics*, *213*(2), 366-386.

Xie, F., Li, L., Pu, Y., Wang, B., Xue, W., Qiu, X., & Wang, G. (2023). Quantifying parametric uncertainty effects on tropical cloud fraction in an AGCM. *Journal of Advances in Modeling Earth Systems*, 15(4), e2022MS003221.

Xie, P., & Arkin, P. A. (1997). Global precipitation: A 17-year monthly analysis based on gauge observations, satellite estimates, and numerical model outputs. *Bulletin of the american meteorological society*, *78*(11), 2539-2558.

Yang, B., Guo, Z., Song, F., Zhang, Y., Zhou, T., & Qian, Y. (2023). Fast and slow responses of atmospheric energy budgets to perturbed cloud and convection processes in an atmospheric global climate model. *Geophysical Research Letters*, *50*(20),

e2023GL104305.

Yang, B., Qian, Y., Lin, G., Leung, L. R., Rasch, P. J., Zhang, G. J., et al. (2013). Uncertainty quantification and parameter tuning in the CAM5 Zhang-McFarlane convection scheme and impact of improved convection on the global circulation and climate. *Journal of Geophysical Research: Atmospheres*, *118*(2), 395-415.

Yang, B., Zhang, Y., Qian, Y., Huang, A., & Yan, H. (2015). Calibration of a convective parameterization scheme in the WRF model and its impact on the simulation of East Asian summer monsoon precipitation. *Climate Dynamics*, *44*, 1661-1684.

Yang, S., & Smith, E. A. (2008). Convective–stratiform precipitation variability at seasonal scale from 8 yr of TRMM observations: Implications for multiple modes of diurnal variability. *Journal of Climate*, *21*(16), 4087-4114.

Zhang, G. J., & McFarlane, N. A. (1995). Sensitivity of climate simulations to the parameterization of cumulus convection in the Canadian Climate Centre general circulation model. *Atmosphere-ocean*, *33*(3), 407-446.

Zhang, G. J., & Mu, M. (2005). Effects of modifications to the Zhang-McFarlane convection parameterization on the simulation of the tropical precipitation in the National Center for Atmospheric Research Community Climate Model, version 3. *Journal of Geophysical Research: Atmospheres*, *110*(D9).

Zhang, G. J., & Song, X. (2010). Convection parameterization, tropical Pacific double ITCZ, and upper-ocean biases in the NCAR CCSM3. Part II: Coupled feedback and the role of ocean heat transport. *Journal of Climate*, *23*(3), 800-812.

Zhang, H., Xie, S. P., Seager, R., & Zhao, S. (2024). Dynamical constraint on precipitation biases over the Indo-Pacific region during boreal summer in AMIP6 models. *Geophysical Research Letters*, *51*(6), e2023GL107181.

Zhang, X., He, B., Guo, Z., Sexton, D. M., Rostron, J. W., & Furtado, K. (2023). Sensitivities of the Asian Summer Monsoon Simulations to Physical Parameters for the Perturbed Parameter Ensemble of HadGEM3-GC3. 05. *Geophysical Research Letters*, *50*(10), e2022GL101826.

Zhao, C., Liu, X., Qian, Y., Yoon, J., Hou, Z., Lin, G., et al. (2013). A sensitivity study of

735 radiative fluxes at the top of atmosphere to cloud-microphysics and aerosol parameters in
736 the community atmosphere model CAM5. *Atmospheric Chemistry and Physics*, *13*(21),
737 10969-10987.
738 Zhou, S., Huang, G., & Huang, P. (2020). Excessive ITCZ but negative SST biases in the
739 tropical Pacific simulated by CMIP5/6 models: The role of the meridional pattern of SST
740 bias. *Journal of Climate*, *33*(12), 5305-5316.